Soft Matter

Dynamic Article Links

Cite this: *Soft Matter*, 2012, **8**, 9792

www.rsc.org/softmatter

PAPER

Thermal transport in single silkworm silks and the behavior under stretching

Guoqing Liu,[a] Xiaopeng Huang,[a] Yuanjing Wang,[b] Yu-Qing Zhang[b] and Xinwei Wang*[a]

Received 17th May 2012, Accepted 9th July 2012
DOI: 10.1039/c2sm26146d

This work reports on the first time study of thermal transport in the axial direction of single silkworm silks. The measured thermal diffusivity of relaxed silkworm silk and thermal conductivity are 0.39×10^{-6} to 2.03×10^{-6} $m^2 s^{-1}$ and 0.54–6.53 W m^{-1} K^{-1}, respectively. The thermal diffusivity of silkworm silk increases up to 263% upon elongation up to 63.8%. For one of the samples studied (sample 5), the thermal conductivity goes up to 13.1 W m^{-1} K^{-1} after elongation of 68.3%, surpassing many other polymers. Three factors combine together to give rise to the remarkable thermal diffusivity increase: alignment improvement of β-sheet blocks, straightening of random coils under stretching, and structural transformation from random coil to β-sheet crystal by elongation (confirmed by our Raman spectroscopy study). Thermal path breakdown is observed when elongation is beyond 63.8%, suggesting that the length of the random coils under relaxed condition is about 61.1% of their real molecular link length. Our Raman spectroscopy study confirms this speculation: after 60% elongation, the Raman frequency started to increase, indicating that the internal strain/stress has been released due to internal structure breakdown.

1. Introduction

Silkworm silk is a fibrous protein composed of two strands of fibroin coated with a layer of sericin. It is widely used and has a lot of advantages like comfort, high mechanical strength and elasticity.[1] The silkworm silk fibroin fibers are about 10–25 μm in diameter. The existing research about silkworm silk is mainly focused on the protein structure,[2–4] mechanical properties and genetics from the viewpoint of biology.[5,6] Many theoretical models have been developed to relate the properties of silkworm silks to their structures.[7,8] Until now the thermal conductivity along the axial direction of silkworm silk has never been reported, largely due to the great difficulty imposed by the small fiber size on measurement. Related work done before is about the silk-cloth's thermal conductivity in the thickness direction.[9] The reported value is about 0.042 W m^{-1} K^{-1}. Because of the contact resistance and porosity among silkworm silk fibers in silk-cloth, the reported thermal conductivity is an effective value of the silk-cloth. According to the silk-cloth producing method, this effective value is largely determined by the radial thermal conductivity of silk. It does not reflect the axial thermal transport capacity of single silkworm silk fibers.

For organic materials, research has offered clear evidence that the thermal conductivity along the direction of molecular orientation will be improved by tensile strain.[10–12] For instance, the thermal conductivity (parallel to the stretching direction) of single crystal mat polyethylene was increased to 41.8 W m^{-1} K^{-1} when the draw ratio is 350 while the thermal conductivity of melt-crystallized polyethylene is about 3 W m^{-1} K^{-1} before stretching. The effect of stretching on the axial and transverse thermal conductivity of polyethylene is different. The axial thermal conductivity is improved as the draw ratio increases, and for transverse thermal conductivity, it is negatively influenced.[13] The anisotropy of thermal conductivity is also observed in linear amorphous high polymers, and the change in tendency of the axial and transverse thermal conductivity caused by stretching is the same as that of single crystal mat polyethylene.[14] A network theory for the thermal conductivity of amorphous polymeric materials has been proposed.[15] In that study, the thermal conductivity of polymers was increased by about 100% when the elongation is 100%. This provides a promising way to improve organic material's thermal conductivity and diffusivity. Silkworm silk has both amorphous regions (which are composed of random coils) and protein crystal regions (primarily β-crystallites) that are highly periodic. Based on the established molecule-spring model,[7] the improvement of thermal transport capability of silkworm silk parallel to the stretching direction is highly expected.

In the past, the single wire 3ω method[16–18] and the micro-fabricated device method[19–23] have been developed to measure the thermal properties of one dimensional structures at the micro/nanoscale. In order to broaden the measurement scope of materials (conductive and nonconductive) and improve the accuracy and stability, we have developed the transient electro-thermal technique (TET) for characterization of thermophysical

[a]*Department of Mechanical Engineering, Iowa State University, Ames, IA, USA 50011. E-mail: xwang3@iastate.edu; Fax: +1 515 294 3261; Tel: +1 515 294 2085*
[b]*Silk Biotechnology Key Laboratory of Suzhou City, Medical College of Soochow University, Suzhou 215123, P. R. China*

properties of micro/nanoscale wires. The TET has been applied to characterize the thermal properties of free-standing micrometer-thick poly(3-hexylthiophene) films,[24] thin films composed of anatase TiO_2 nanofibers,[25] single-wall carbon nanotubes,[26] and micro/sub-microscale polyacrylonitrile wires.[27]

In this work, silkworm silks are hand reeled from cocoons and characterized for their thermal transport capacity under relaxed and stretched conditions. A structural model is established to explain the observed improvement of the thermal diffusivity and thermal path breakdown. Raman analysis is performed to study the structure change of the silkworm silk under large elongation, in anticipation to understand the physics behind the thermal diffusivity increase.

2. Materials and methods

2.1. Sample preparation

The *Bombyx mori* cocoon is boiled in water at about 100 °C for several minutes. We use a small wooden rod to stir the water, and silks will twist and stick to the rod. The length of the silk we get by this hand-reeling method could be as long as 1 m. In order to dry the samples, the silk is heated at 140 °C for three hours. Then a silkworm silk sample with a length of 2–3 mm is connected between two copper bases by using silver paste. Because silkworm silk is nonconductive, a gold film of 80 nm is coated on the sample surface to make it electrically conductive.

This is our first study of thermal properties of silkworm silk along the axial direction, so we would like to keep the sample as original as possible. Our next research step will be focused on degummed single fiber of fibroin.

2.2. Thermal characterization

The TET technique[26] is an efficient approach to measuring the thermal diffusivity of solid materials, including conductive, semiconductive or non-conductive one-dimensional structures. A schematic of the TET experimental setup is shown in Fig. 1 (bottom). In the TET technique, the sample is suspended between two copper electrodes. A fed current–time (I–t) profile and an induced voltage–time (V–t) profile recorded by the oscilloscope are presented in Fig. 1 (top). In order to simplify the model to one dimensional, the length of the wire should be much longer than its diameter and more details can be referred to Guo's work.[26] With the resistance change ΔR during the transient state and the calibrated temperature coefficient of resistance η (which equals dR/dT), the steady state average temperature rise ΔT is calculated and then the thermal conductivity (k) is obtained as $k = I^2RL/(12A\Delta T)$. Here A and L are the cross-sectional area and length of the gold-coated wire, respectively. The normalized temperature rise (T^*) is solved for a one-dimensional heat transfer problem as:

$$T^* = \frac{96}{\pi^4}\sum_{m=1}^{\infty}\frac{1-\exp\left[-(2m-1)^2\pi^2\alpha t/L^2\right]}{(2m-1)^4}. \quad (1)$$

The voltage evolution (V_{wire}) recorded by the oscilloscope is directly related to the average temperature change of the silkworm silk as:

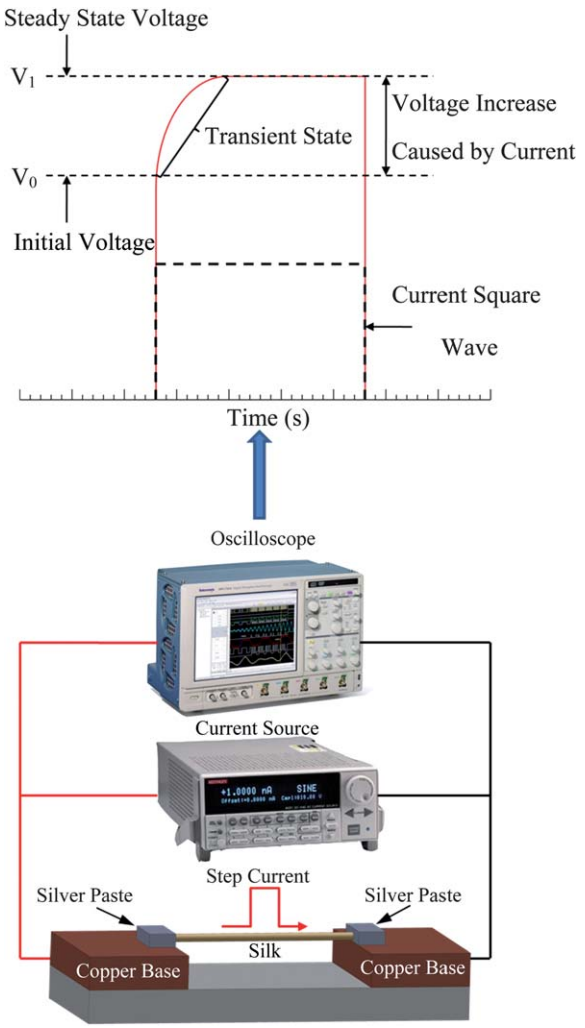

Fig. 1 (Top) Fed current (black dashed line) and methodology to determine the thermophysical properties based on the resulted V–t profile (red solid line) and (bottom) schematic of the experimental principle and the step current provided for the TET.

$$V_{wire} = IR_0 + I\eta\frac{q_0L^2}{12k}\times T^*. \quad (2)$$

R_0 is the resistance of the silkworm silk before heating. q_0 is the electrical heating power per unit volume. It is clear that the measured voltage change is inherently related to the temperature change of the silkworm silk. The measured thermal diffusivity (α_e) is only an effective value combining both effects of the silkworm silk and the gold coating because the tested silkworm silk is already coated with a thin gold film. The thermal transport effect caused by the coated layer can be subtracted using the Wiedemann–Franz law with negligible increase of the uncertainty. The real thermal diffusivity (α) of the silkworm silk is determined as:[26]

$$\alpha = \alpha_e - \frac{L_{Lorenz}TL}{RA(\rho c_p)_e}, \quad (3)$$

where ρ and c_p are the effective density and the specific heat of the sample, respectively, and L_{Lorenz} is the Lorenz number. The real thermal conductivity can also be determined following a similar methodology and is derived as:

$$k = k_e - \frac{L_{Lorenz} TL}{RA}. \quad (4)$$

In order to determine the real thermal diffusivity using eqn (3) and thermal conductivity using eqn (4), the density and specific heat are required. We have $(\rho c_p)_e = k_e/\alpha_e$, then based on eqn (3) and (4), the real thermophysical properties are obtained. In ref. 26, Guo used A_w (the cross-sectional area of the original wire before gold film coating), instead of A, in eqn (3) and (4) to subtract the thermal transport effect caused by the coated layer. Actually, because the coated gold film is very thin (nanometers scale), the difference between the calculation results by using A_w and A is negligible. In eqn (3) and (4), the thermal transport in the gold-coated silk has to be dominated by the silk in order to have sound accuracy when subtracting the effect of the gold film. In our experiment, the gold film is very thin (tens of nm), much smaller than the silk thickness. Our further data processing also confirmed that the thermal transport is dominated by that in the silk.

3. Results and discussion

3.1. Measurement of thermophysical properties

First of all, we discuss the TET measurement of sample 1 to provide the idea on how the measurement is conducted and analyzed. In the TET technique, the sample is suspended between two copper electrodes. During the experiment, a step dc current is fed through the wire (gold-coated sample) to introduce electrical heating. The temperature increase history of the sample is closely related to the heat transfer along it. The temperature change of the sample will cause a resistance change, which can change the voltage over the wire. So the temperature change of the sample will be monitored by measuring the voltage variation over it. Once the temperature evolution is obtained, the thermal diffusivity of the wire can be obtained by fitting the normalized temperature evolution curve against time. Since silkworm silk is non-conductive, a thin film of gold is coated on its surface to make it conductive. As discussed in Guo's work,[26] theoretical fitting of the normalized experimental temperature rise [expressed by eqn (1)] is conducted by using different trial values of the thermal diffusivity of the sample. The value giving the best fit of the experimental data is taken as the property of the fiber. Fitting of the experimental data for sample 1 is shown in Fig. 2. Its thermal diffusivity is determined at 0.45×10^{-6} m^2 s^{-1}, which includes the influence of the gold coating layer. For comparison, two curves of different thermal diffusivity values are also plotted in Fig. 2, one is 1.06α and the other is 0.94α. The fitting uncertainty is about $\pm 6\%$.

To subtract the effect of gold coating on thermal transport and obtain the real thermal properties, the sample size needs to be determined. A scanning electron microscope (SEM) is used to study the sample size, like length, layer thickness of sericin and the radius of fibroin. Fig. 3 shows the SEM images of sample 1. Its length is 2.605 mm, and the diameter of a single fibroin fiber is about 12 μm. Because the silk is composed of two fibroin fibers and sericin covering them, a model has been established to simplify the calculation and calculate the cross-sectional area of the silk based on the SEM images.

The simplified geometry configuration of the silkworm silk is illustrated in Fig. 3(c), and we have:

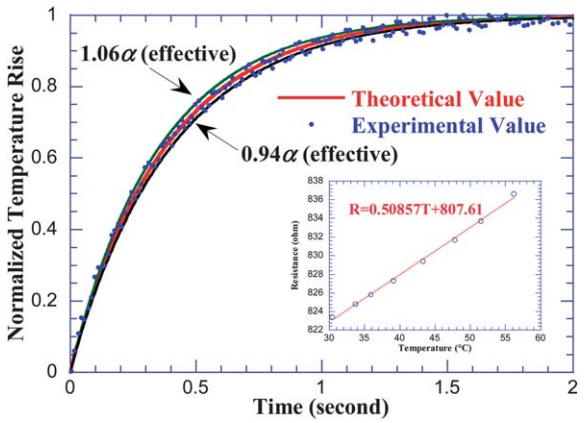

Fig. 2 Comparison between the theoretical fitting and experimental data for the normalized temperature rise *versus* time (silkworm silk sample 1) and linear fitting curve of the temperature coefficient of resistance for the silkworm silk sample 1.

$$\beta = \cos^{-1}\left(\frac{r + d/2}{r + d}\right), \quad (5)$$

$$S = (r + d)\left[\pi(r + d)\left(2 - \frac{\beta}{180}\right) - \left(r + \frac{d}{2}\right)\sin\beta\right], \quad (6)$$

here β stands for the angle shown in Fig. 3(c) and S has the same value as A in eqn (3) and (4). From Fig. 2(b), according to our cross-section structure, the values of 26.51, 26.31 and 26.18 μm represent the summation of $4r + 3d$. In Fig. 2(b) (inset), the small flake on the surface of the silkworm silk should be sericin, which means during the hand-reeling process, some of the sericin may be dissolved in water. It is evaluated that the average value of r is 6.10 μm, so the thickness of the sericin layer d is 0.64 μm. For sample 5, by using the same method, we obtained d and r, but for samples 2, 3, and 4, it is very difficult to find a part not covered with sericin, so $d = 0.64$ μm is used to calculate r by deducting it from $4r + 3d$. The effect of the uncertainty of the thickness of the sericin layer on thermal parameters' analysis is almost negligible. The cross-sectional areas of the five measured samples are detailed in Table 1. Their fibroin fiber radius is 6.1, 6.08, 6.66, 5.49, and 5.73 μm for samples 1 to 5, respectively, showing a quite uniform silk diameter from sample to sample.

The thermal conductivity of the sample is calculated from the calibration procedure and the steady state TET temperature rise. The calibration result of silkworm silk sample 1 is displayed in Fig. 2 (inset). The temperature–resistance relationship is linear, similar to a metallic conductor. This is because the electrical conduction of the silkworm silk is sustained by the gold coating. The temperature coefficient of resistance, which is 0.51 Ω K^{-1} for sample 1, is obtained by linear fitting of the calibration result [Fig. 2 (inset)]. During the experiment, a 0.3 mA DC was fed through this sample, the resistance change was 12.22 Ω and the consequent temperature rise was 24.04 K. The thermal conductivity is derived based on the expression $k = I^2RL/(12A\Delta T)$ as 2.45 W m^{-1} K^{-1}, which includes the influence of the gold coating layer, radiation and rarefied gas conduction in the chamber. A series of experiments have been conducted in our lab to calibrate the effect of radiation and gas conduction using glass fibers. Based on the glass fiber calibration, for sample 1, the effect of

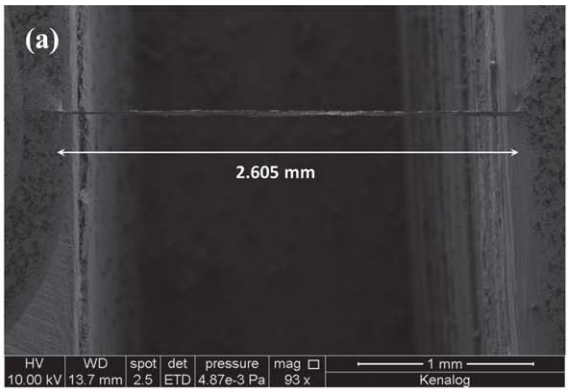

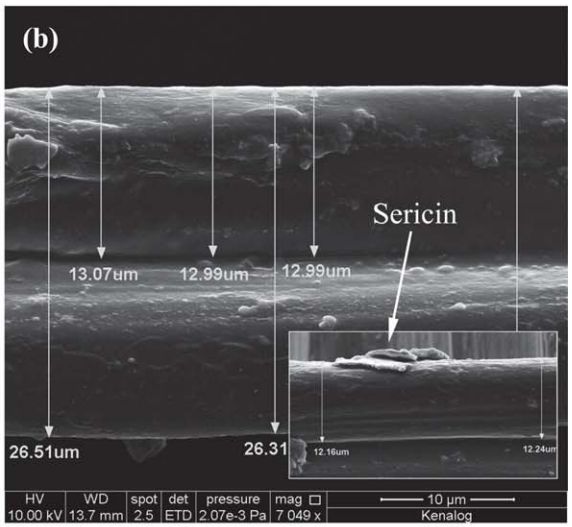

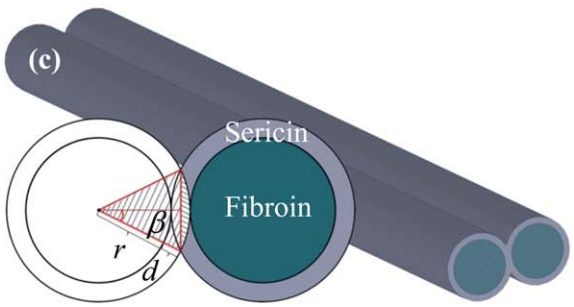

Fig. 3 SEM pictures, structural model (3D) and cross-section (2D) of silkworm silk sample 1. (a) The length of the sample connected between copper bases. (b) The silkworm silk (*Bombyx mori*) composed of two strands of fibroin coated with sericin. The inset in (b) shows that part of the sericin is dissolved in water during the hand-reeling process. (c) Structural model (3D) and cross-section (2D) of silkworm silk. The outside layer (in grey) and inner layer (in dark green) stand for sericin and fibroin, respectively.

radiation and gas conduction on the thermal conductivity is 1.83 W m^{-1} K^{-1}. Therefore the effective thermal conductivity is 0.62 W m^{-1} K^{-1}. More details about the radiation and rarefied gas conduction will be described in our later publications. By using $\alpha = k/\rho c_p$, we can obtain ρc_p (effective), then apply eqn (3) and (4) to calculate the real thermal diffusivity, conductivity and the volume-based specific heat. The detailed parameters and calculation results for sample 1 are listed in Table 2.

3.2. Thermal conductivity and diffusivity of relaxed silkworm silk

Details of experimental parameters and results for the five silkworm silk samples are summarized in Table 1. The thermal diffusivity and conductivity of silkworm silk vary from 0.39 $\times$ 10^{-6} to 2.03 $\times$ 10^{-6} m^2 s^{-1} and 0.54–6.53 W m^{-1} K^{-1}, respectively. It is apparent that the silkworm silk has a better conductivity compared with other polymers, such as cotton (0.06 W m^{-1} K^{-1}, at 300 K), leather (sole) (0.159 W m^{-1} K^{-1} at 300 K), rubber (vulcanized) (soft, 0.13 W m^{-1} K^{-1}, at 300 K; hard, 0.16 W m^{-1} K^{-1}, at 300 K),[28] PMMA ($\sim$0.20 W m^{-1} K^{-1}, at 300 K),[29] and polycarbonate ($\sim$0.21 W m^{-1} K^{-1}, at 300 K),[30] but not as good as Kevlar 49 ($\sim$30 W m^{-1} K^{-1}, at 300 K). As mentioned above, the thermal conductivity of silk-cloth in the thickness direction is about 0.042 W m^{-1} K^{-1}.[9] It is obvious that this result cannot fully reveal the sound thermal transport capability of silkworm silk because of the contact resistance, porosity between the fibers and the difference of the thermal properties in the thickness and axial directions. From Table 1, it is noticed that the volume-based specific heat is very consistent except for sample 3. Probably this exceptional value is induced by the different structure of this section of the silk or large experimental uncertainty for this sample. The average value of ρc_p for samples 1, 2, 4 and 5 is 1.36 $\times$ 10^6 J m^{-3} K^{-1}. From Table 1, the average cross-sectional area of samples 1, 2, 4, and 5 is 269 μm^2. In the next we will use 1.36 $\times$ 10^6 J m^{-3} K^{-1} and 269 μm^2 for thermal parameters analysis under stretching. In this way, there is no need to perform the calibration procedure which is difficult for the experiment under stretching. Actually, the cross-sectional area may change a little in the elongation process, but this parameter is only used for subtracting the effect of gold when calculating the real thermal diffusivity and conductivity by applying eqn (3) and (4). After consideration and comparison, the difference caused by this simplification is almost negligible. Take sample 5 as an example, the real cross-sectional area, effective thermal diffusivity and real thermal diffusivity are 277 μm^2, 0.86 $\times$ 10^{-6} m^2 s^{-1} and 0.83 $\times$ 10^{-6} m^2 s^{-1}, respectively. If we assume ρc_p changes from 1.65 $\times$ 10^6 J m^{-3} K^{-1} to 1.36 $\times$ 10^6 J m^{-3} K^{-1}, the real thermal diffusivity will change to 0.82 $\times$ 10^{-6} m^2 s^{-1}, which means the 17.6% difference of ρc_p only induces 1.2% change of the real thermal diffusivity. In the same way, if the cross-sectional area changes to 200 μm^2, the real thermal diffusivity will change to 0.82 $\times$ 10^{-6} m^2 s^{-1}. 27.8% difference of the cross-sectional area also only gives 1.2% change of the real thermal diffusivity. So it is reasonable and convenient to use the average value of ρc_p and the average cross-sectional area, which is 1.36 $\times$ 10^6 J m^{-3} K^{-1} and 269 μm^2, for the thermal parameters analysis of elongated silkworm silk in the next section.

3.3. Effect of stretching on thermal conductivity and thermal diffusivity

Seven silkworm silk samples are characterized by using the TET twice: one with the original length, and the other one with the elongated length. We used a spring-control device to stretch the silkworm silk. Generally speaking it will take about 10 seconds to do that. And not every sample can be elongated so large and the successful rate is very low for large elongations. Because the gold

Table 1 Details of experimental parameters and results for five silkworm silk samples characterized by using the TET and calibration technique

Sample	Length (mm)	Cross-sectional area (μm^2)	$\Delta R/\Delta T$ ($\Omega\ K^{-1}$)	ρc_p (real) ($\times 10^6$ J m^{-3} K^{-1})	α (real) ($\times 10^{-6}$ m^2 s^{-1})	k (real) (W m^{-1} K^{-1})
1	2.61	284	0.51	1.37	0.39	0.54
2	2.91	282	0.94	1.18	2.03	2.39
3	2.62	333	1.04	3.66	1.78	6.53
4	2.98	234	0.57	1.23	0.90	1.10
5	2.59	277	0.86	1.65	0.83	1.37

Table 2 Details of experimental parameters and results for silkworm silk sample 1 characterized by using the TET and calibration technique

Length (mm)	2.61
Cross-sectional area (μm^2)	284
Resistance (before TET) (Ω)	844.17
Resistance (after TET) (Ω)	856.39
DC current (mA)	0.3
Effective thermal diffusivity ($\times 10^{-6}$ m^2 s^{-1})	0.45
Real thermal diffusivity ($\times 10^{-6}$ m^2 s^{-1})	0.39
Effective thermal conductivity (W m^{-1} K^{-1})	0.62
Real thermal conductivity (W m^{-1} K^{-1})	0.54
ρc_p (effective) ($\times 10^6$ J m^{-3} K^{-1})	1.37
ρc_p (real) ($\times 10^6$ J m^{-3} K^{-1})	1.37

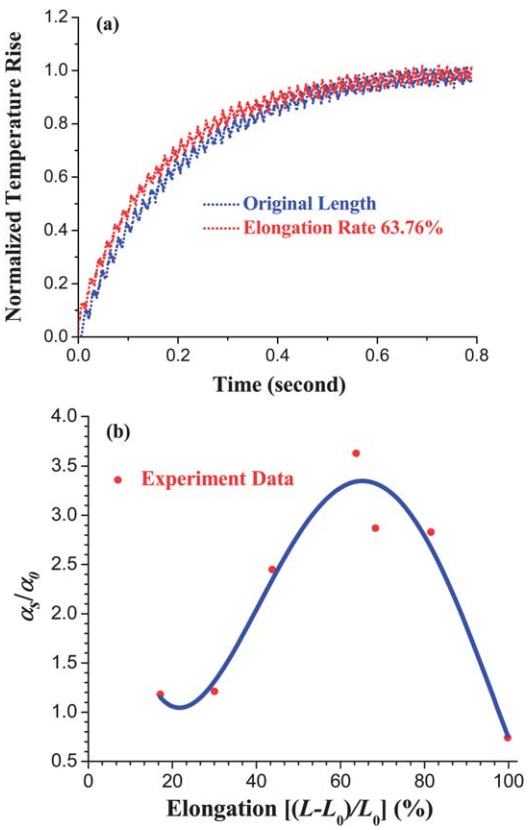

Fig. 4 (a) The normalized temperature rise for the silkworm silk with the original length and elongated length. (b) The ratio of thermal diffusivity under different elongation. α_0 and α_s are the thermal diffusivity (after subtraction of the effect of the gold) of the same silkworm silk sample with the original length and elongated length, respectively. Here elongation = $(L - L_0)/L_0$, L stands for the length after elongation and L_0 is the original length. The blue curve is used to guide eyes for the trend of data variation.

film on the surface of the sample broke in the elongation process, the sample was coated with 80 nm of gold film again after stretching to guarantee its conductivity. Considering the variation of thermal diffusivity from sample to sample, the ratio of the thermal diffusivity after stretching to that before stretching for each sample is used to study the elongation effect.

With the purpose of showing the magnificent effect of elongation on thermal properties, the fitting curves of the thermal diffusivity (effective) of the silkworm silk with the original length and elongated length (elongated by 63.76%) are shown in Fig. 4(a). From Fig. 4(a) it is noticed that even after elongation, it takes a shorter time for the sample to reach the steady state in the TET measurement. Considering the fact that the thermal diffusivity is proportional to L^2/t_c, where L is the sample length and t_c the characteristic time to reach the steady state, even without fitting we can directly conclude from the raw experimental data that after elongation of 63.76%, the thermal diffusivity should increase by at least 168% over that of relaxed silk. Such an increase is just magnificent and very exciting. If considering the shorter t_c after stretching, this increase will be even larger and is discussed in the following section. Silkworm silk offers a choice of flexible material for heat transfer. Silkworm silk can be embedded into other low-thermal-conductivity materials to increase the capacity of thermal transport while providing the excellent bio-compatible interface. We believe this material should be very promising and may be used in many fields such as flexible electronics and bio-sensors.

The exact experiment results of the seven elongated samples are shown in Table 3. α_0 and α_s are the thermal diffusivity (after the subtraction of the gold coating effect) of the same silkworm silk at the original length and elongated length, respectively. Because of the variation of thermal diffusivity of different silkworm silk samples, even when obtained from the same cocoon, it makes more sense to use the ratio of thermal diffusivity under different elongation to observe the effect of elongation on the thermal parameters. In Fig. 4(b), the blue curve is used to guide eyes to view the data trend. It is clearly shown that the thermal diffusivity is largely improved by elongation initially, then reaches a peak, and finally drops. Our observation is that when the elongation reaches about 63.8%, the thermal diffusivity, increasing up to 263%, reaches the maximum value/increase.

For silkworm silk, decided by the biological structure and our stretching method, it is difficult to get a draw ratio larger than 2 (elongated by 100%). So the final thermal diffusivity increase is not as much as some polymers, such as single crystal mat polyethylene and gel polyethylene.[13] But under the same stretching ratio (~63.8%), the silkworm silk has a relatively large thermal diffusivity increase. For poly(methyl methacrylate), the thermal

Table 3 Details of experimental parameters and results for seven elongated silkworm silk samples characterized by using the TET

Sample	Original length (mm)	α_0 ($\times 10^{-6}$ m^2 s^{-1})	Elongated length (mm)	α_s ($\times 10^{-6}$ m^2 s^{-1})	Elongation (%)	α_s/α_0
1	2.35	2.34	2.75	2.77	17.15	1.18
2	1.97	1.64	2.56	1.98	30.05	1.21
3	2.04	1.75	2.94	4.29	43.74	2.45
4	2.41	1.69	3.95	6.13	63.76	3.63
5	2.56	3.36	4.31	9.64	68.31	2.87
6	1.93	1.34	3.50	3.79	81.45	2.83
7	2.13	2.34	4.26	1.74	99.81	0.74

conductivity is only increased by less than 10% (at 313 K) under the same stretching.[12,30] For polycarbonate, the thermal conductivity is increased by about 78% (at 425 K).[30] Here we introduce a concept of speed of thermal diffusivity increase by stretching as $\zeta = [d(\alpha_e/\alpha_0)/d((L - L_0)/L_0)]$. It can be conveniently used to assess how easy/difficult the thermal transport capability can be improved by stretching. For silkworm silk, ζ is very large (about 4) when the elongation is from 30 to 50%. When the elongation is ~63.8%, the thermal diffusivity reaches the maximum, and ζ becomes zero. For poly(methyl methacrylate), ζ is only 0.13 (at 313 K);[12] for polycarbonate, ζ is 1.12 (at 425 K).[30] For single crystal mat polyethylene, ζ is only 0.16 (at 295 K).[13]

With further elongation, the thermal diffusivity starts to decrease quickly against stretching, indicating breakdown of the thermal transport path in the silk although the silk does not break yet as seen from outside. For other polymers mentioned above, ζ is always positive, which means under stretching, the thermal diffusivity increase ratio is becoming larger and larger, and no thermal transport path breakdown is observed. For the data shown in Table 3, after stretching, the thermal diffusivity increases to a higher level. For sample 5, the thermal diffusivity is 9.64×10^{-6} m^2 s^{-1} at the elongation of 68.31%, which is the largest one in the seven samples. Applying the average value of ρc_p, which is 1.36×10^6 J m^{-3} K^{-1}, the thermal conductivity is estimated to be 13.1 W m^{-1} K^{-1}. This value is very high compared with that of the polymers mentioned above. It indicates broader applications of silkworm silk in terms of heat dissipation. For other polymers, after stretching, the thermal transport in the direction normal to the stretching direction is reduced.[12,13] At present, it is still very challenging to measure the thermal diffusivity/conductivity of single silkworm silk in the radial direction. But it is expected the silkworm silk should have the same phenomenon that its thermal transport capability in the radial direction will be reduced significantly by stretching.

3.4. Physics behind the improvement of thermal transport capacity by elongation

A molecular-spring model[7] is established to explore the mystery of the silkworm silk structure [Fig. 5(a)] and to explain the elongation effect on the thermal properties in the axial direction. The biological structure of silks can be divided into crystalline (primarily the β-crystallites, which are also a kind of β-sheet structure) and non-crystalline (amorphous) domains, which contain random coils.[31] Take the angle of inclination of the β-sheets as θ [shown in Fig. 5(b)], and neglect the thermal transportation between strands of β-sheets, from the viewpoint of thermal transport, then for the β-sheet blocks we have

$$\frac{\Delta T}{L} kA = \frac{\Delta T}{L\cos\theta} k_{\text{eff}} \frac{A}{\cos\theta}, \tag{7}$$

here ΔT, L, k, k_{eff}, A and θ are temperature difference, the average length of β-sheet block, average thermal conductivity in the chain direction of β-sheet block, effective thermal conductivity in the axial direction of the silk, the cross-sectional area and the average inclination angle. Then we have $k_{\text{eff}} = k\cos^2\theta$. So when θ is 90 degrees, the average thermal conductivity in the chain direction will not contribute to the thermal transport in the axial direction of the silkworm silk. Instead, the weak thermal transport among strands will contribute to the thermal transport in the silk axial direction. In the past, it has been proved that in polymers, the thermal transport along the molecular chain direction is much larger than that in the transverse direction.[13] This is attributed to

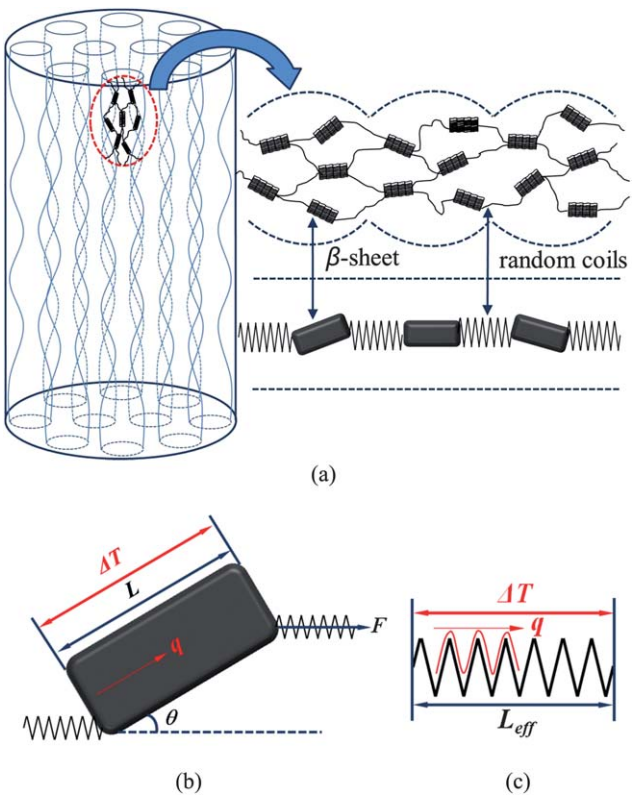

Fig. 5 (a) The model of the silkworm silk structure. The block and string stand for β-sheet and the random coils. (b) Schematic of thermal transport along the β-sheet crystal. L is the length of the crystal, F the force applied on the silkworm silk during elongation, and θ the angle of inclination. (c) Schematic of thermal transport along the random coils. L_{eff} is the effective length of the spring. q in (b) and (c) stands for the heat flux direction.

the fact that vibration (phonons) is easy to transfer along molecular chains rather than from chain to chain.

Similarly, for the spring model of random coils [shown in Fig. 5(c)], we have

$$\frac{\Delta T}{L_{\text{tot}}} kA = \frac{\Delta T}{L_{\text{eff}}} k_{\text{eff}} A_{\text{eff}}, \tag{8}$$

here ΔT, L_{tot}, L_{eff}, k, k_{eff}, A and A_{eff} are temperature difference, the average total length of the spring, average effective length of the spring, average thermal conductivity, effective thermal conductivity, the cross-sectional area and the effective cross-sectional area. A_{eff} should have a linear relationship with the ratio of L_{tot} and L_{eff}, then we have $k_{\text{eff}} = H(L_{\text{eff}}/L_{\text{tot}})^2$, here H is a constant coefficient.

When the elongation ranges from 0% to about 60%, the effective thermal conductivity of β-sheet blocks will be improved as the inclination angle decreases because of stretching [in eqn (7)]. This is because under external stretching, the β-sheet crystals will change their orientation to be more aligned along the stretching direction. For random coils, because of the increase of the L_{eff} [in eqn (8)] under stretching, the thermal conductivity of this part has also improved a lot. After the peak (when elongation is about 68%) in Fig. 4(b), more elongation will cause breakage of the inner bonds, leading to breakdown of some random coils. As a result, some β-sheet crystals will lose the external stretching, and their inclination angle θ will become larger again, like that at the relaxed state. This will not contribute to the improvement of the thermal conductivity any more. Based on our observation in Fig. 4(b), at the elongation of ~64%, the thermal diffusivity starts to decrease, meaning breakdown of the random coils. Since the orientation change of the β-sheet crystal will have very limited contribution to length change (unless the crystal has a large aspect ratio), we can conclude that the 64% elongation largely comes from the random coils straightening. The breakage of the thermal transport path at 64% elongation leads to one very important conclusion: the length of the random coils under relaxed condition is about 61.1% of their true straight molecular length. When the elongation arrives at about 100%, the silkworm silk will break at any time.

3.5. Explanation of the improvement of thermal properties after elongation based on Raman spectroscopy

Raman spectra of the silkworm silk under different elongation are studied using a confocal Raman spectrometer (Voyage, BWTek, Inc.) coupled with an Olympus BX51 microscope. It employs a 532 nm green laser with 20 mW power as the excitation light source. The beam is focused with a 50× objective which gives a laser power of about 8 mW on the sample. A sample of silkworm silk is placed over the two legs of a digital caliper and glued with silver paste. The caliper is used to stretch the silk at different elongation until breaking. In order to focus the beam point at almost the same place on the silk after stretching, the caliper is fixed on a precision 3D (XYZ) positioning stage (562 Series ULTRAlign™, Newport) and the stage can offset the original place back to the beam point. It will take about 5 to 30 minutes to focus the laser on the silkworm silk sample, so during this period, the stretched sample will relax (structure stabilizes under the tension). The spectra are collected over the silk at different elongation for an integration period of 20 seconds. No visible silk degradation occurred under the selected experimental conditions. Spectra are corrected for the fluorescence background over the 500–3000 cm^{-1} spectral region by subtracting a polynomial baseline. They are then smoothed by using the Savitzky–Golay method with eight points. Wave number shifts due to experimental conditions of the spectrometer are corrected using the tyrosine band at 1615 cm^{-1} like others did in the literature.[32] There are several main peaks in the Raman plot (Fig. 6), like Peak 1 at 1082 cm^{-1} (νCC skeletal stretching in β-sheet and random coil), and Peak 2 at 1242 cm^{-1} (amide III).[33] Shoulder and peak positions for β-sheet, which are near 1260 cm^{-1} and 1630 cm^{-1}, are shown in Fig. 6. The relationship between elongation and Raman frequency is obtained and shown in Fig. 6 (inset).

In Fig. 6, spectral changes induced by elongation are plotted. The spectrum before the treatment is apparently ascribable to the random coil structure. After elongation, due to the β-sheet structure, additional bands, a shoulder at 1260 cm^{-1} and a peak at 1630 cm^{-1}, emerged.[34] Under different elongation, from 0% to 100%, the shoulder at 1260 cm^{-1} appears, and the peak at 1630 cm^{-1} becomes sharper. Because the laser we used in this experiment is not polarized, the chance that these observations are caused by the improved orientation of the β-sheet with respect to the fiber axis is small. This leads to an important conclusion: the structure transforms from the random coil to β-sheet by stretching/elongation. This transformation partly contributes to the improvement of thermal diffusivity since the crystal phase is expected to have a higher thermal conductivity than the amorphous phase. This phenomenon is also observed in other polymers under stretching. For single crystal mat polyethylene, the crystallinity can increase from 0.831 to 0.845, when the draw ratio is 6, to 0.932, when the draw ratio is 350. For gel polyethylene, the crystallinity can increase from 0.818 to 0.926 when the draw ratio is 200.[13]

Generally speaking, for polymer materials, when the strain increases, the stress in the material will increase, and this will cause the decrease of the wave number. At the same time, the

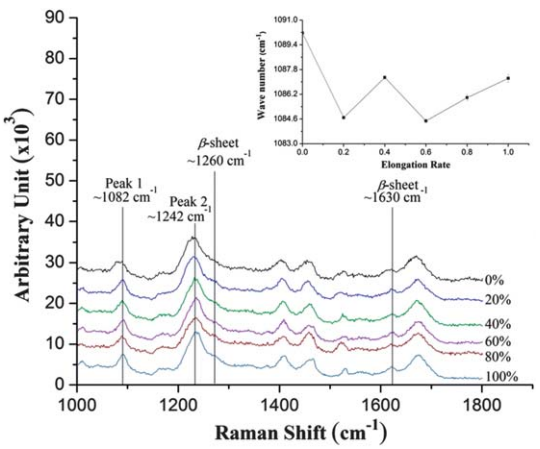

Fig. 6 Raman shift changes of fibroin after elongation: peak positions for β-sheet are near 1260 cm^{-1} and 1630 cm^{-1}. The relationship between Raman shift and elongation for Peak 1 is shown in the inset. In the Raman spectrum, Peak 1 (~1082 cm^{-1}) is for νCC skeletal stretching in β-sheet and random coil, and Peak 2 (~1242 cm^{-1}) is for amide III.

thermal conductivity of polymer materials will be negatively affected under strains. From Fig. 6 (inset), it is apparent that, when the elongation is less than 20%, the Raman frequency is decreasing. The existence of the internal stress will enhance phonon scattering, making the thermal conductivity/diffusivity smaller. However, for silkworm silk, this effect is significantly offset by the alignment effect of the β-sheet crystal and random coils. Therefore we only observe a thermal diffusivity increase. If we combine Fig. 6 (inset) and Fig. 4(b), we can conclude that when the elongation is about 60%, the wave number reaches its lowest value and the ratio of the thermal diffusivity arrives at its peak. After this point, the Raman frequency begins to increase and the ratio of the thermal diffusivity decreases with the increase of elongation. Our previous speculation based on the observation in Fig. 4(b) is that the thermal diffusivity decrease after 64% elongation is because of the breakdown of the random coils. Such speculation can be further confirmed by the observation in Fig. 6 (inset). After 60% elongation, it is observed that the Raman frequency starts to increase. This means the internal strain/stress has been released partly even when the silk is stretched. Such strain/stress release can only be attributed to internal structure breakdown. We believe that there are many uncertainties in Raman experiment results reported here. The up-down variation of the Raman peak position could also be caused by unknown experimental uncertainties. So the above argument is not extremely strong. Higher-resolution Raman spectroscopy with highly controlled environment is needed in future research for studying the structural evolution under stretching.

4. Conclusion

In this work, thermal transport in the axial direction of single silkworm silks was characterized for the first time. The thermal diffusivity of silkworm silk without elongation varied from 0.39 $\times 10^{-6}$ to 2.03 $\times 10^{-6}$ $m^2 s^{-1}$, and the thermal conductivity was in a range of 0.54–6.53 W m^{-1} K^{-1}. Compared with other polymers, the thermal conductivity of silkworm silks is very high. The thermal diffusivity of silkworm silk was largely improved when elongated to about 60%. Under 63.8% elongation, the thermal diffusivity was observed to have an increase of 263%, meaning that the thermal diffusivity of silkworm silk under elongation is more than three times that at the original length. So it is easy to achieve large manipulation of thermal transportation. For one of the samples studied (sample 5), after elongation of 68.31%, the thermal conductivity was estimated to be 13.1 W m^{-1} K^{-1}. The decrease of the inclination angle of the β-sheet blocks, the increase of the effective length of the spring model of random coils, and the transformation from the random coil to β-sheet by elongation contributed to the improvement of thermal diffusivity. When the silkworm silk was elongated beyond 64%, more and more inner bonds were broken, which caused the decrease of thermal diffusivity. The breakage of the thermal transport path at 64% elongation leads to one very important conclusion: the length of the random coils under relaxed condition was about 61.1% of their real molecular link length. Our Raman spectroscopy study of the silkworm silk under elongation also confirmed this speculation. After 60% elongation, the Raman frequency started to increase. This means the internal strain/stress has been released even when the silk is stretched. Such strain/stress release can only be attributed to internal structure breakdown.

Acknowledgements

Partial support of this work from the National Science Foundation (CBET-0931290, CMMI-0926704, CBET-0932573) and Office of Naval Research (N000141210603) is gratefully acknowledged.

References

1 T. Asakura, R. Sugino, J. M. Yao, H. Takashima and R. Kishore, *Biochemistry*, 2002, **41**, 4415–4424.
2 C. Z. Zhou, F. Confalonieri, N. Medina, Y. Zivanovic, C. Esnault, T. Yang, M. Jacquet, J. Janin, M. Duguet, R. Perasso and Z. G. Li, *Nucleic Acids Res.*, 2000, **28**, 2413–2419.
3 K. Yamaguchi, Y. Kikuchi, T. Takagi, A. Kikuchi, F. Oyama, K. Shimura and S. Mizuno, *J. Mol. Biol.*, 1989, **210**, 127–139.
4 S. Inoue, K. Tanaka, F. Arisaka, S. Kimura, K. Ohtomo and S. Mizuno, *J. Biol. Chem.*, 2000, **275**, 40517–40528.
5 D. Kaplan, W. W. Adams, B. Farmer and C. Viney, *Silk Polymers*, 1994, vol. 544, pp. 2–16.
6 J. Sirichaisit, V. L. Brookes, R. J. Young and F. Vollrath, *Biomacromolecules*, 2003, **4**, 387–394.
7 X. Wu, X. Y. Liu, N. Du, G. Q. Xu and B. W. Li, *Appl. Phys. Lett.*, 2009, **95**, 093703.
8 V. I. Lim and S. V. Steinberg, *FEBS Lett.*, 1981, **131**, 203–207.
9 E. S. Rood, *Phys. Rev.*, 1921, **18**, 356–361.
10 K. H. Hellwege, W. Knappe and J. Hennig, *Acta Vet. Acad. Sci. Hung.*, 1963, **13**, 121–127.
11 D. Hands, *Rubber Chem. Technol.*, 1980, **53**, 80–87.
12 B. D. Washo and D. Hansen, *J. Appl. Phys.*, 1969, **40**, 2423–2427.
13 C. L. Choy, Y. W. Wong, G. W. Yang and K. Tetsuo, *J. Polym. Sci., Part B: Polym. Phys.*, 1999, **37**, 3359–3367.
14 B. D. Washo and D. Hansen, *J. Appl. Phys.*, 1969, **40**, 2423.
15 B. H. A. A. Vandenbrule, *Rheol. Acta*, 1989, **28**, 257–266.
16 L. Lu, W. Yi and D. L. Zhang, *Rev. Sci. Instrum.*, 2001, **72**, 2996–3003.
17 T. Y. Choi, D. Poulikakos, J. Tharian and U. Sennhauser, *Nano Lett.*, 2006, **6**, 1589–1593.
18 J. B. Hou, X. W. Wang, P. Vellelacheruvu, J. Q. Guo, C. Liu and H. M. Cheng, *J. Appl. Phys.*, 2006, **100**, 124314–124319.
19 P. Kim, L. Shi, A. Majumdar and P. L. McEuen, *Phys. Rev. Lett.*, 2001, **87**, 215502.
20 P. Kim, L. Shi, A. Majumdar and P. L. McEuen, *Physica B*, 2002, **323**, 67–70.
21 L. Shi, D. Y. Li, C. H. Yu, W. Y. Jang, D. Y. Kim, Z. Yao, P. Kim and A. Majumdar, *J. Heat Transfer*, 2003, **125**, 881–888.
22 D. Y. Li, Y. Y. Wu, P. Kim, L. Shi, P. D. Yang and A. Majumdar, *Appl. Phys. Lett.*, 2003, **83**, 2934–2936.
23 L. Shi, Q. Hao, C. H. Yu, N. Mingo, X. Y. Kong and Z. L. Wang, *Appl. Phys. Lett.*, 2004, **84**, 2638–2640.
24 X. H. Feng and X. W. Wang, *Thin Solid Films*, 2011, **519**, 5700–5705.
25 X. Feng, X. Wang, X. Chen and Y. Yue, *Acta Mater.*, 2011, **59**, 1934–1944.
26 J. Q. Guo, X. W. Wang and T. Wang, *J. Appl. Phys.*, 2007, **101**, 063537.
27 J. Q. Guo, X. W. Wang, L. J. Zhang and T. Wang, *Appl. Phys. A: Mater. Sci. Process.*, 2007, **89**, 153–156.
28 F. P. Incropera, D. P. DeWitt and T. L. Bergman, *Fundamentals of Heat and Mass Transfer*, John Wiley, Hoboken, NJ, 2007, pp. 939–940.
29 K. Eiermann and K. H. Hellwege, *J. Polym. Sci., Part B: Polym. Phys.*, 1962, **57**, 99–106.
30 C. L. Choy, W. P. Leung and Y. K. Ng, *J. Polym. Sci., Part B: Polym. Phys.*, 1987, **25**, 1779–1799.
31 A. H. Simmons, C. A. Michal and L. W. Jelinski, *Science*, 1996, **271**, 84–87.
32 T. Lefevre, M. E. Rousseau and M. Pezolet, *Biophys. J.*, 2007, **92**, 2885–2895.
33 P. Colomban, H. M. Dinh, J. Riand, L. C. Prinsloo and B. Mauchamp, *J. Raman Spectrosc.*, 2008, **39**, 1749–1764.
34 Y. Tsuboi, T. Ikejiri, S. Shiga, K. Yamada and A. Itaya, *Appl. Phys. A: Mater. Sci. Process.*, 2001, **73**, 637–640.